

Strong shock in the uniformly expanding universe with a spherical void

G.S. Bisnovatyi-Kogan^{1,2,3*}, S.A. Panafidina^{1,3†}

¹Space Research Institute RAS, Moscow, Russia;

²National Research Nuclear University MEPhI, Moscow, Russia;

³Moscow Institute of Physics and Technology MIPT, Moscow reg., Russia

Abstract

Propagation of strong shock wave in the expanding universe is studied using approximate analytic, and exact numerical solution of self-similar equations. Both solutions have similar properties, which change qualitatively, depending on the adiabatic powers γ . In the interval $1 < \gamma < \gamma_{cr} \sim 1.16$ analytic and numeric solutions fill all the space without any voids and they are rather close to each other. At larger $\gamma > \gamma_{cr}$ a pressure becomes zero at finite radius, and a spherical void appears around the origin in both solutions. All matter is collected in thin layer behind the shock wave front. The structure of this layer qualitatively depends on γ . At the inner edge of the layer the pressure is always zero, but the density on this edge is jumping from zero to infinity at $\gamma \approx 1.4$ in both solutions.

Keywords: cosmology, strong shock wave, self-similar solution

*Email: gkogan@iki.rssi.ru

†Email: sofya.panafidina@phystech.edu

1 Introduction

Strong explosions could happen at stages of star and galaxy formation, and at last stages of evolution of very massive primordial stars. Observations of GRB optical afterglows have shown existence of heavy elements in the universe at red shifts up to $z \sim 10$, like in GRB090423 at $z \approx 8.2$, GRB120923A at $z \approx 8.5$, GRB090429B with a photo- $z \approx 9.4$ [1]. The heavy elements should be formed in the explosions at earlier stages, at larger red shifts. Strong explosions are accompanied by formation of a strong shock wave, propagating in the expanding universe. For a static media propagation of strong shocks was studied by many authors, see e.g. [2],[3]. Exact analytic solution of self-similar equations, describing strong shock propagation was obtained by L.I. Sedov [4, 5]. Similar analytic solution was obtained in [6], for a strong explosion in the expanding media of a flat Friedman dust universe [7]. Contrary to the static media, which has a real zero energy density in the undisturbed state, the zero energy density in the flat Friedman dust universe, in Newtonian approximation, is the result of a sum of the positive kinetic, and negative gravitational energies. This balance could be lost behind the shock, therefore the analytic solution obtained using the integral of motion similar to [4], is an approximate one. Here we obtain approximate analytic, and exact numerical solutions for the strong shock propagation for a gas at different adiabatic powers γ .

It was obtained that numerical solutions, where matter fills the whole space, exist only at $\gamma < \gamma_{cr} = \gamma_* \approx 1.155$. Similar properties are expressed by the approximate analytic solutions with $\gamma_{cr} = \gamma_* \approx 1.178$.

The problem of a strong shock propagation in the expanding medium was considered earlier in different approximations in [8]- [14]. Review of papers on this topic is given in [15]. Propagation of a detonation wave in the flat expanding universe was studied in [16, 17]. Shock propagation in the outflowing stellar wind was considered in [18].

Detailed analysis of solutions with $\gamma > \gamma_{cr}$ revealed a fundamental difference of the structure of a thin layer near the shock. The pressure at the inner edge of the layer is zero, but density is changing from zero to infinity when γ reaches the value $\gamma = \gamma_{cr1} \approx 1.4$. It is the same within numerical errors in numerical and analytical solutions, while the density inside this layer has a quite different behaviour.

2 Self-similar equations for a strong shock in a uniform expanding medium

Equations describing in the Newtonian approximation, a uniformly expanding $v = H(t)r$, self-gravitating medium, with a density $\rho(t)$ depending only on time, corresponding to the Friedman model of the universe, in spherical coordinates is written as [7]

$$\begin{aligned} \frac{\partial v}{\partial t} + v \frac{\partial v}{\partial r} &= -\frac{1}{\rho} \frac{\partial p}{\partial r} - \frac{G_g m}{r^2}, & \frac{\partial \rho}{\partial t} + \frac{\partial \rho v}{\partial r} + \frac{2\rho v}{r} &= 0, \\ \left(\frac{\partial}{\partial t} + v \frac{\partial}{\partial r} \right) \ln \frac{p}{\rho^\gamma} &= 0, & \frac{\partial m}{\partial r} &= 4\pi \rho r^2, \end{aligned} \quad (1)$$

where G_g is the gravitational constant. We consider a flat dusty model with a zero velocity at time infinity, having a density $\rho_1(t)$, and expansion velocity $v_1 = H_1(t)r$. The solution of the system (1) in these conditions is written as

$$\begin{aligned} \rho_1 = \delta/t^2, \quad \delta = \frac{1}{6\pi G_g}, \quad \rho_1 = \frac{1}{6\pi G_g t^2}; \quad H_1 = \frac{2}{3t}, \quad v_1 = 2r/3t; \\ m = \frac{4\pi}{3} \rho r^3 = \frac{2r^3}{9G_g t^2}, \quad \frac{G_g m}{r^2} = \frac{2}{9} \frac{r}{t^2}. \end{aligned} \quad (2)$$

The Newtonian solution is physically relevant in the region where $v_1 \ll c_{\text{light}}$, $c \ll c_{\text{light}}$. In the case of a point explosion with the energy E , at $t = 0$, the number of parameters is the same as in the static medium (δ, E) , therefore we may look in this case for a self-similar solution in the problem of a strong shock propagation.

The non-dimensional combination in this case is written as $r(\delta/Et^4)^{1/5}$. A position of the shock in the self-similar solution corresponds to the fixed value of the self-similar coordinate. The distance of the shock to the center R is written as

$$R = \beta \left(\frac{Et^4}{\delta} \right)^{1/5}, \quad (3)$$

where β is a parameter depending only on the adiabatic power γ . The velocity of the shock u in the static laboratory frame is written as

$$u = \frac{dR}{dt} = \frac{4R}{5t} = \frac{4\beta E^{1/5}}{5\delta^{1/5}t^{1/5}}. \quad (4)$$

The shock propagation velocity u , the velocity of the matter behind the shock v_2 , in the uniformly expanding medium (2), are decreasing with time $\sim t^{-1/5}$, the pressure behind the shock p_2 is decreasing $\sim t^{-2/5}$, which is slower than in the case of the constant density medium. It occurs due to the fact, that the background density is decreasing with time, and the resistance to the shock propagation is decreasing also.

Conditions on the strong shock discontinuity (Hugoniot relations) has the following view

$$\begin{aligned} v_2 &= \frac{2}{\gamma+1}u + \frac{\gamma-1}{\gamma+1}v_1^{sh}, \quad \rho_2 = \frac{\gamma+1}{\gamma-1}\rho_1, \\ p_2 &= \frac{2}{\gamma+1}\rho_1(u - v_1^{sh})^2, \quad c_2^2 = \frac{2\gamma(\gamma-1)}{(\gamma+1)^2}(u - v_1^{sh})^2, \end{aligned} \quad (5)$$

where $v_1^{sh} = \frac{2R}{3t}$ is the unperturbed expansion velocity on the shock level. The subscript "2" is related to the values behind the shock. Introduce non-dimensional variables behind the shock as

$$v = \frac{4r}{5t}V, \quad \rho = \frac{\delta}{t^2}G, \quad c^2 = \frac{16r^2}{25t^2}Z, \quad m = \frac{4\pi}{3}\rho_1 r^3 M = \frac{4\pi}{3} \frac{r^3}{t^2} \delta M, \quad (6)$$

depending on the self-similar variable ξ , written as

$$\xi = \frac{r}{R(t)} = \frac{r}{\beta} \left(\frac{\delta}{Et^4} \right)^{1/5}. \quad (7)$$

In non-dimensional variables (6), the conditions (5) on the strong shock at $r = R$, $\xi = 1$, are written as

$$V(1) = \frac{5\gamma + 7}{6(\gamma + 1)}, \quad G(1) = \frac{\gamma + 1}{\gamma - 1}, \quad Z(1) = \frac{\gamma(\gamma - 1)}{18(\gamma + 1)^2}, \quad M(1) = 1, \quad (8)$$

and the system (2) is written as

$$Z \left(\frac{d \ln Z}{d \ln \xi} + \frac{d \ln G}{d \ln \xi} + 2 \right) + \gamma(V - 1) \frac{dV}{d \ln \xi} = \gamma V \left(\frac{5}{4} - V \right) - \frac{25}{72} \gamma M, \quad (9)$$

$$\frac{dV}{d \ln \xi} - (1 - V) \frac{d \ln G}{d \ln \xi} = -3V + \frac{5}{2}, \quad (10)$$

$$\frac{d \ln Z}{d \ln \xi} - (\gamma - 1) \frac{d \ln G}{d \ln \xi} = -\frac{5 - 2V - \frac{5}{2}\gamma}{1 - V}, \quad (11)$$

$$\xi \frac{dM}{d\xi} = 3(G - M). \quad (12)$$

The relations used here are

$$\left. \frac{\partial \xi}{\partial t} \right|_r = -\frac{4\xi}{5t}, \quad \left. \frac{\partial \xi}{\partial r} \right|_t = \frac{\xi}{r}. \quad (13)$$

A constant β in the definition of the non-dimensional radius ξ in (7) is obtained from the explosion energy integral E . Due to zero energy (kinetic + gravitational) in the non-perturbed solution, the conserving value of the explosion energy behind the shock, in the uniformly expanding medium, with velocity and density distributions (2), with account of the gravitational energy, is determined as

$$E = \int_0^{R(t)} \rho \left[\frac{v^2}{2} + \frac{c^2}{\gamma(\gamma - 1)} \right] 4\pi r^2 dr - \int_0^{R(t)} \frac{G_g m dm}{r}. \quad (14)$$

In non-dimensional variables (6) this relation reduces to the equation for the constant β

$$\beta^{-5} = \frac{64\pi}{25} \int_0^1 G \left[\frac{V^2}{2} + \frac{Z}{\gamma(\gamma - 1)} \right] \xi^4 d\xi - \frac{8}{3} \int_0^1 G \xi \left(\int_0^\xi G \eta^2 d\eta \right) d\xi. \quad (15)$$

3 Approximate analytic solution

3.1 Approximate first integral

Using the procedure described in [19] for the case of the shock in a static media, it was possible to obtain an approximate energy conservation integral in the expanding medium of the universe [6], in the form

$$Z = \frac{(\gamma - 1)(1 - V)(V - \frac{5}{6})^2}{2(V - \frac{5}{6} - \frac{1}{6\gamma})}. \quad (16)$$

At the shock $r = R$, $\xi = 1$, using $Z(1)$ and $V(1)$ from (8), the approximate first integral gives an identity. Using (16) we may consider only two differential equations (10) and (11), for finding an analytical solution of the problem, similar to the classical Sedov case. The relation (16) may be interpreted as a happy choice of the profiling function for the temperature distribution behind the shock.

3.2 Approximate analytic solution for expanding medium

Excluding Z from equations (10),(11) with the help of (16), the analytic solution of self-similar system of equations (9)-(12) was obtained in [6, 20] in the form

$$\left[(\gamma + 1)(3V - \frac{5}{2}) \right]^{\mu_1} \left[\frac{\gamma + 1}{\gamma - 1}(6\gamma V - 5\gamma - 1) \right]^{\mu_2} \left[6(\gamma + 1) \frac{3\gamma V - V - \frac{5}{2}}{15\gamma^2 + \gamma - 22} \right]^{\mu_3} = \xi, \quad (17)$$

with

$$\begin{aligned} \mu_1 &= \frac{2}{15\gamma - 20}, \quad \mu_2 = \frac{\gamma - 1}{17\gamma - 15\gamma^2 + 1}, \\ \mu_3 &= -\frac{\gamma + 1}{3\gamma - 1} - \frac{\gamma - 1}{17\gamma - 15\gamma^2 + 1} + \frac{2}{20 - 15\gamma}. \end{aligned} \quad (18)$$

$$G(V) = \frac{\gamma + 1}{\gamma - 1} \left[6 \frac{(\gamma + 1)(1 - V)}{\gamma - 1} \right]^{\kappa_1} \left[\frac{\gamma + 1}{\gamma - 1}(6\gamma V - 5\gamma - 1) \right]^{\kappa_2} \quad (19)$$

$$\times \left[\frac{3(\gamma + 1)}{15\gamma^2 + \gamma - 22} [(6\gamma - 2)V - 5] \right]^{\kappa_3}.$$

Here

$$\begin{aligned} \kappa_1 &= \frac{7}{3\gamma - 1} - \frac{2}{6\gamma - 7} + \frac{(15\gamma - 20)(\gamma - 1)}{(6\gamma - 7)(15\gamma^2 - 17\gamma - 1)} \\ &\quad - \frac{3\gamma(15\gamma - 20)}{(3\gamma - 1)(15\gamma^2 - 17\gamma - 1)} - \frac{15\gamma - 20}{3\gamma - 1} \frac{\gamma + 1}{6\gamma - 7}, \\ \kappa_2 &= -\frac{3}{3\gamma - 1} + \frac{3\gamma(15\gamma - 20)}{(3\gamma - 1)(15\gamma^2 - 17\gamma - 1)}. \\ \kappa_3 &= \frac{2}{6\gamma - 7} - \frac{(15\gamma - 20)(\gamma - 1)}{(6\gamma - 7)(15\gamma^2 - 17\gamma - 1)} + \frac{15\gamma - 20}{3\gamma - 1} \frac{\gamma + 1}{6\gamma - 7}. \end{aligned} \quad (20)$$

The function $Z(V)$ is determined by the integral (16). Here the boundary conditions (8) at $\xi = 1$ have been used.

$$M(\xi) = 3\xi^{-3} \int_0^\xi G(\eta)\eta^2 d\eta. \quad (21)$$

4 Main properties of the approximate analytic solution

4.1 Approximate analytic solution at γ less than critical value

The analytic solution (17),(19),(16),(21) has a complicated dependence of γ , and physically relevant solution exists only for limited values on γ . In order to have positive values in brackets of (17), and to satisfy the condition for V on the shock (8) we obtain restrictions for V as

$$V > \frac{5}{6}, \quad V > \frac{1 + 5\gamma}{6\gamma}, \quad V < V(1) = \frac{5\gamma + 7}{6(\gamma + 1)}. \quad (22)$$

To satisfy all these conditions we obtain the restriction for γ as $1 < \gamma < \gamma_*$, where γ_* is defined by equation

$$15\gamma^2 + \gamma - 22 = 0, \quad \gamma_* = -\frac{1}{30} + \sqrt{\frac{1}{900} + \frac{22}{15}}, \quad \gamma_* \approx 1.1782. \quad (23)$$

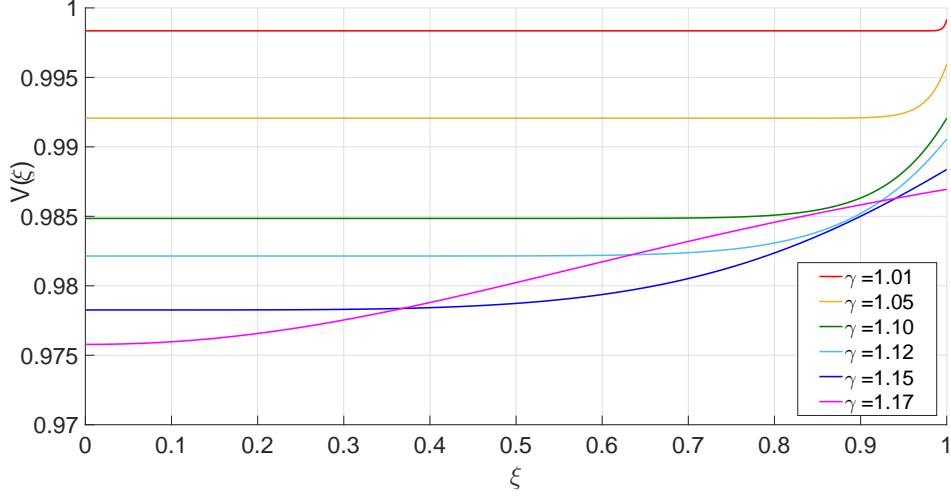


Figure 1: Approximate analytic solution without voids for $V(\xi)$

Numerical solutions of self-similar equations (9)-(12), presented below, have similar restrictions for γ . We may conclude, therefore, that for other $\gamma > \sim \gamma_*$ there are no smooth self-similar solutions in the whole space. On figures are plotted, for different $\gamma < \gamma_*$, functions from the analytical solution: $V(\xi)$ from (17) in Fig.1; $G(\xi)$ from (19) in Fig.2; $Z(\xi)$ from (16) in Fig.3; and $M(\xi)$ from (21) in Fig.4.

Introduce notations

$$V' = \frac{dV}{d\xi}, \quad G' = \frac{dG}{d\xi}, \quad Z' = \frac{dZ}{d\xi} \quad (24)$$

At the shock $\xi = 1$ the derivative of the self-similar functions are found from the analytic solution (17)-(19) in the form [20]

$$V'(1) = \frac{-15\gamma^2 - \gamma + 22}{6(\gamma + 1)^2}; \quad G'(1) = \frac{-15\gamma^2 + 5\gamma + 28}{(\gamma - 1)^2};$$

$$Z'(1) = \frac{(15\gamma^2 + \gamma - 22)\gamma}{9(\gamma + 1)^3}. \quad (25)$$

It follows from (23),(25), that for $\gamma < \gamma_*$ the derivatives have the following signs

$$V'(1) > 0; \quad G'(1) > 0; \quad Z'(1) < 0 \quad (26)$$

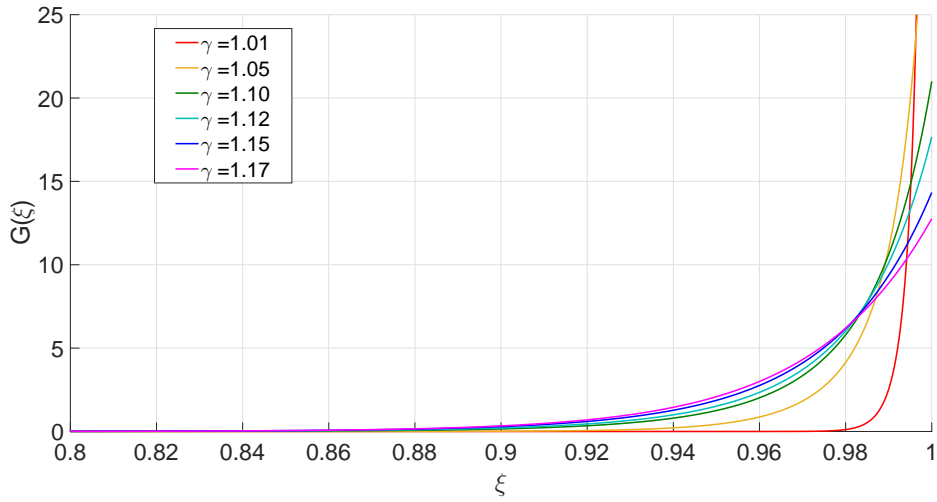


Figure 2: Approximate analytic solution without voids for $G(\xi)$

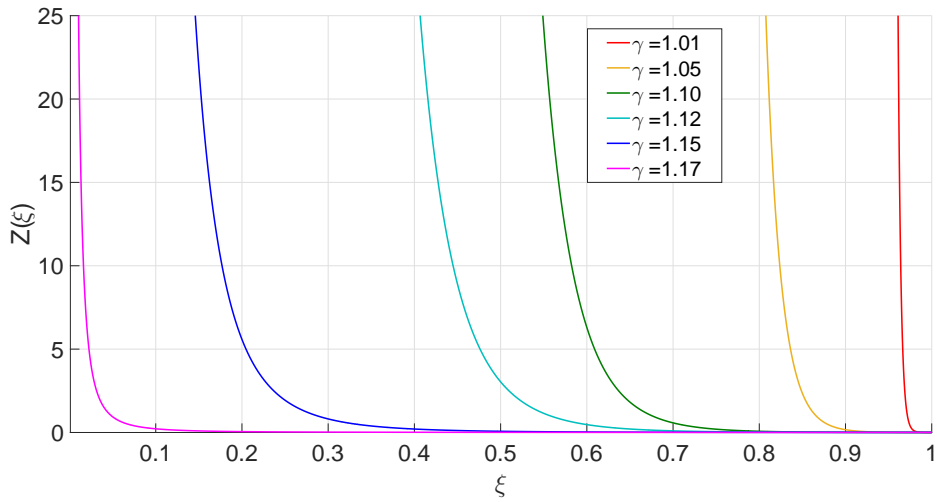


Figure 3: Approximate analytic solution without voids for $Z(\xi)$

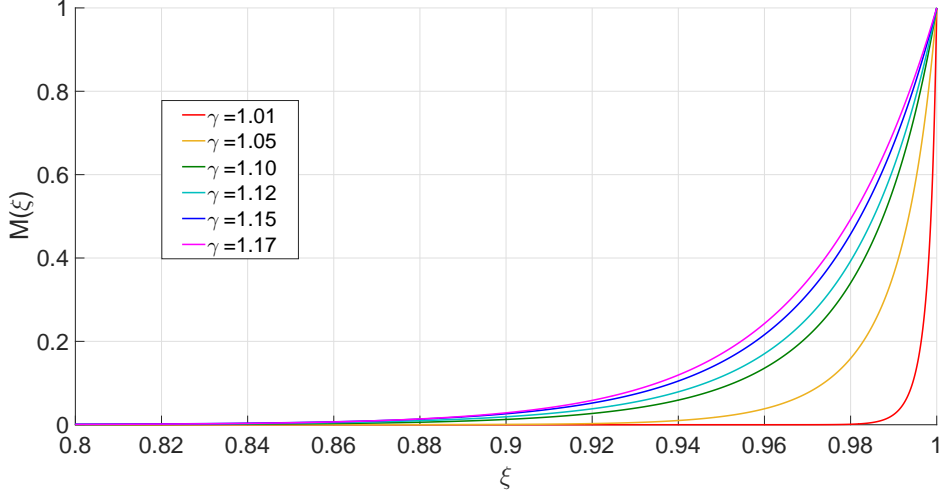


Figure 4: Solution without voids for $M(\xi)$ from (21) based on approximate analytic equations

4.2 Approximate analytic solution at γ larger than critical value

Consider approximate analytic solution at $\gamma \geq \gamma_* \approx 1.1782$. Contrary to the approximate analytic solution for $V(\xi)$ at $\gamma < \gamma_*$, the function $V(\xi)$ increases up to infinity at $\xi \rightarrow 0$.

It follows from (19) that $G(\xi)$ has a physical sense only when $V(\xi) < 1$, because $V(\xi) = 1$ is the point where $G(\xi) = 0$. That means that there is a point where density of matter becomes zero and spherical void area appears. Dependence of radius ξ of such spherical void areas on γ can be written in the form

$$\left[\frac{\gamma+1}{2}\right]^{\mu_1} \left[\gamma+1\right]^{\mu_2} \left[3(\gamma+1)\frac{6\gamma-7}{15\gamma^2+\gamma-22}\right]^{\mu_3} = \xi, \quad (27)$$

with μ_1, μ_2, μ_3 from Eq.(18).

Calculation of self-similar variables, using Eqs. (17),(19) gives, that at the point with $V = 1$ the density goes to zero at $\gamma < \gamma_{cr1} = 1.4$, and for larger γ the density tends to infinity at this point. Nevertheless, the temperature goes to zero at this point, so that the pressure, represented by the function GZ goes to zero

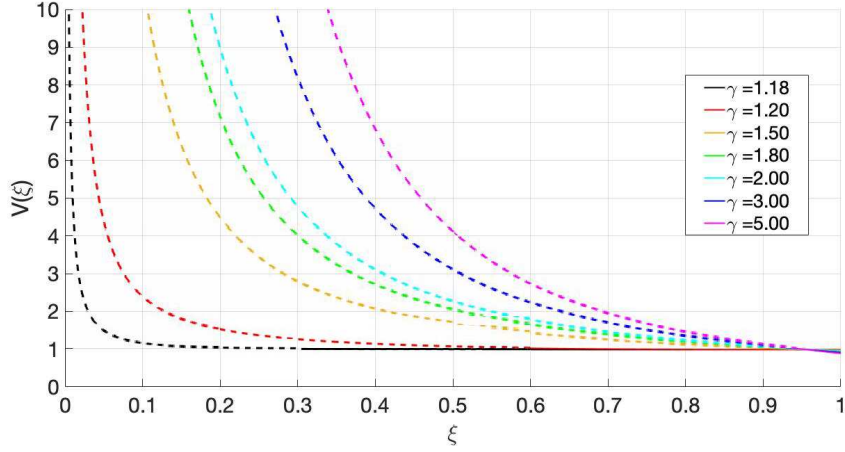


Figure 5: Approximate analytic solution for $V(\xi)$ at $\gamma > \gamma_*$, plotted according to Eq.(17). Non-physical parts of curves at $V \geq 1$ are given by dashed lines.

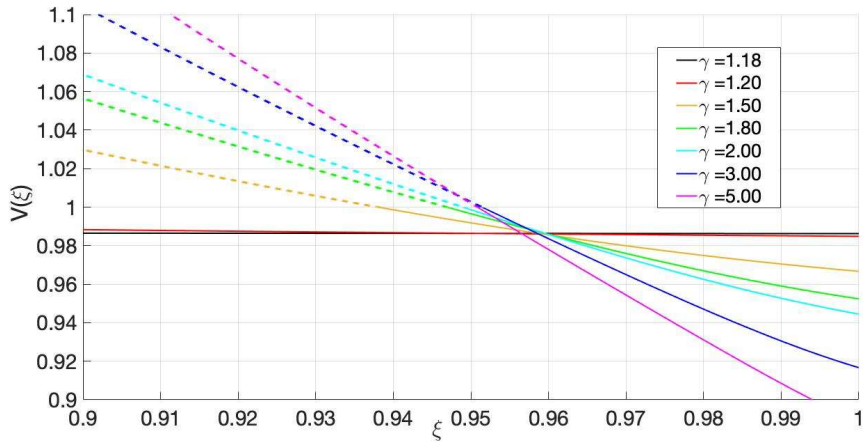


Figure 6: Approximate analytic solution for $V(\xi)$ at $\gamma > \gamma_*$, plotted according to Eq.(17) in the vicinity of the shock. Non-physical parts of curves at $V \geq 1$ are given by dashed lines.

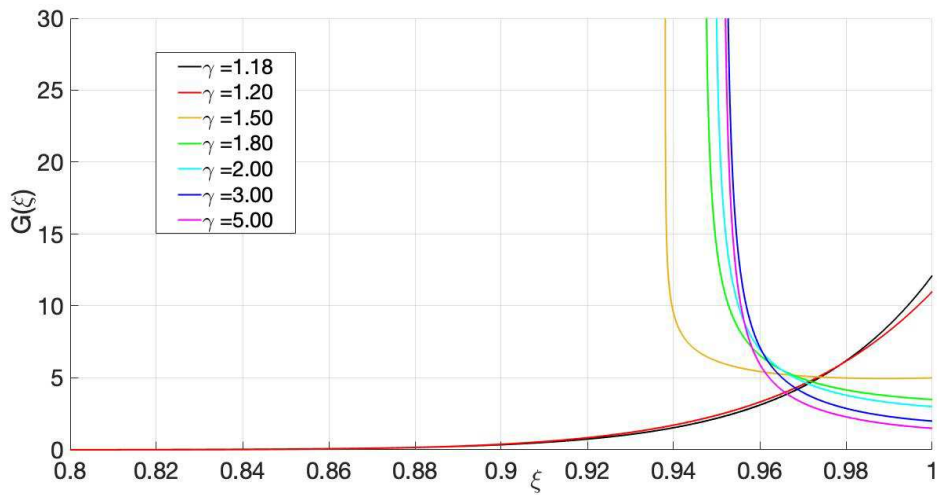


Figure 7: Approximate analytic solution for $G(\xi)$ at $\gamma > \gamma_*$, plotted according to Eqs.(17),(19).

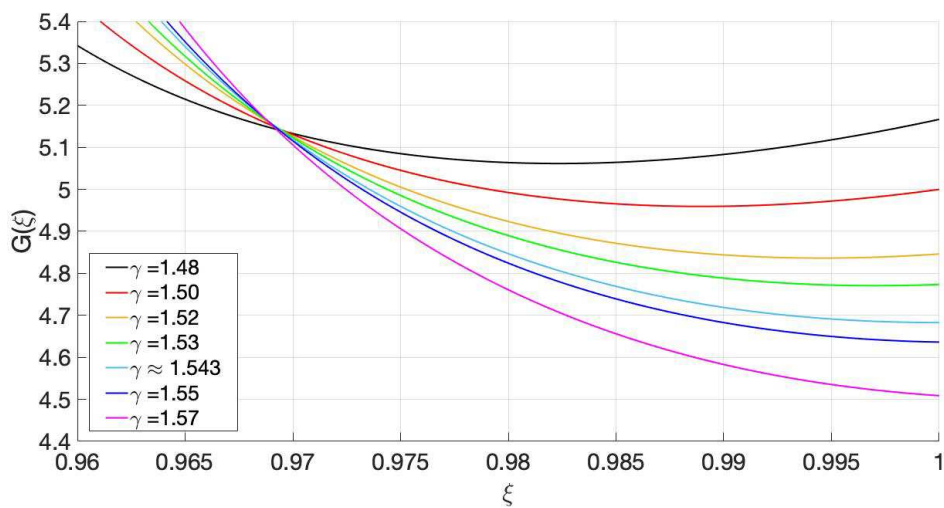


Figure 8: Approximate analytic solution for $G(\xi)$ at $\gamma \approx 1.1543$, in the vicinity of the shock.

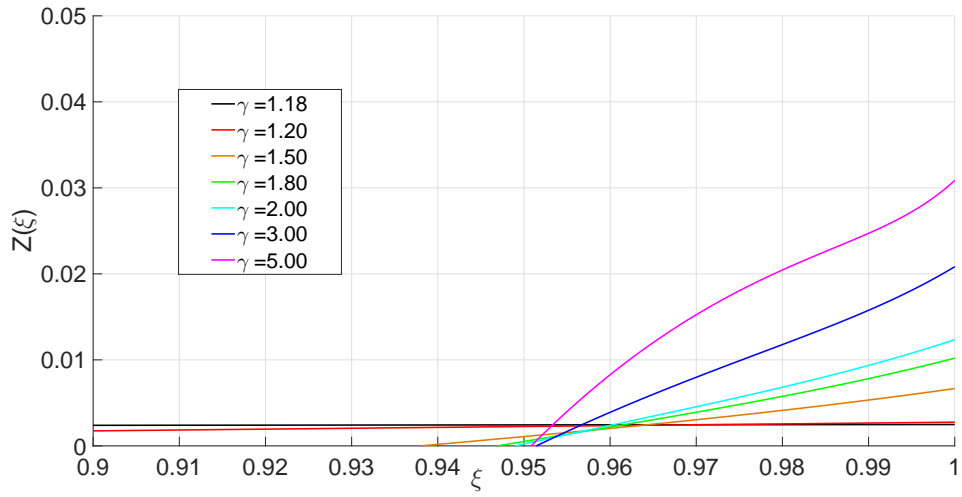


Figure 9: Approximate analytic solution for $Z(\xi)$ at $\gamma > \gamma_*$ plotted according to Eq.(17),(16) in the vicinity of the shock.

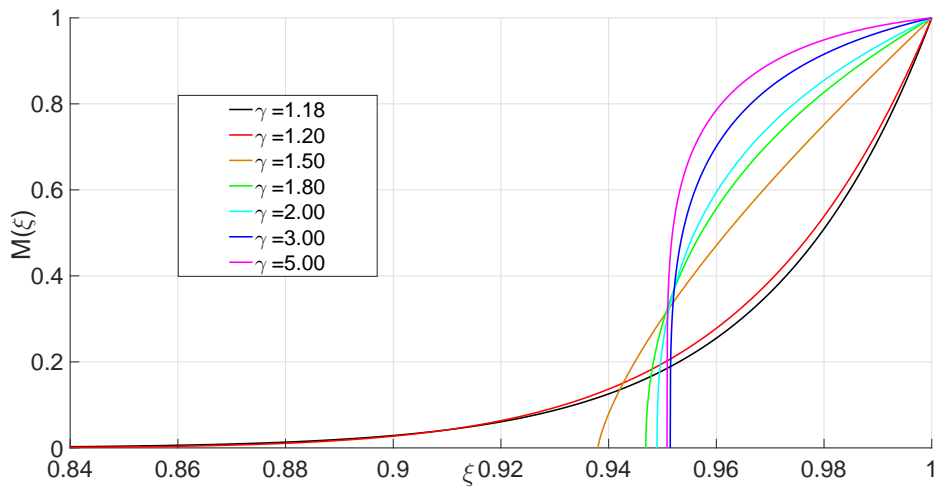


Figure 10: Approximate analytic solution for $M(\xi)$ at $\gamma > \gamma_*$, plotted by integration in Eq.(21) in the vicinity of the shock.

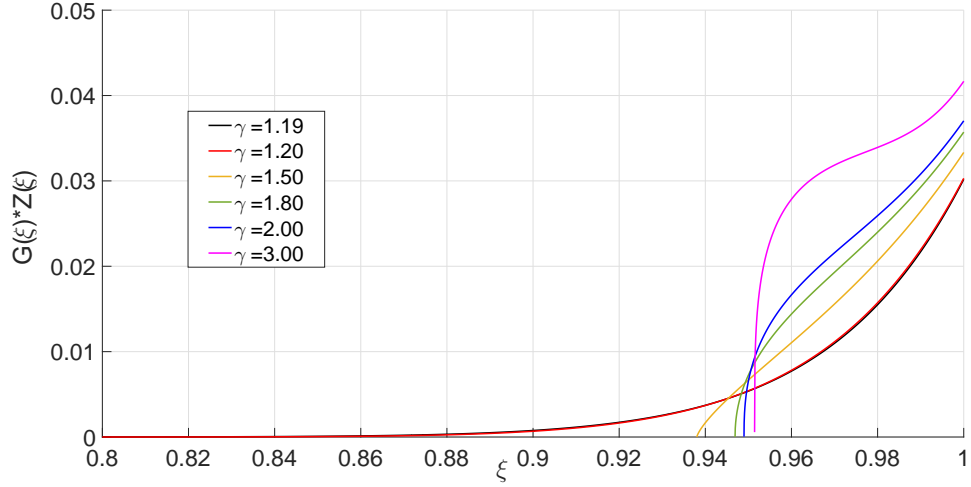


Figure 11: Approximate analytic solution for $G(\xi) * Z(\xi)$ at big γ , in the vicinity of the shock.

at the inner edge of the layer at $V = 1$, so we obtain a self-consistent solution with the spherical void. The following figures represent behaviour of functions at different $\gamma > \gamma_*$: $V(\xi)$ in Figs.(5),(6); $G(\xi)$ in Figs.(7),(8); $Z(\xi)$ in Fig.(9); $M(\xi)$ in Fig.(10); $G(\xi) \times Z(\xi)$ in Fig.(11).

We obtain from (25) that $G'(\xi)|_{\xi=1} > 0$ at $\gamma < \frac{5+\sqrt{1705}}{30} \approx 1.54305$ and $G'(\xi)|_{\xi=1} < 0$ at $\gamma > \frac{5+\sqrt{1705}}{30}$. So the density starts to fall and then rises up to infinity at $1.4 < \gamma < \frac{5+\sqrt{1705}}{30}$. When $\gamma > \gamma_2 = \frac{5+\sqrt{1705}}{30}$ the density starts to grow inside from the shock, and continues rising up to infinity.

5 Numerical solution of self-similar equations

5.1 Numerical solution at γ less than critical value

The system of equations (9)-(12) written explicitly for derivatives has a form:

$$\begin{cases} \frac{d \ln G}{d \ln \xi} = \frac{\frac{3-\frac{5}{2}\gamma}{1-V}Z - \frac{25}{72}\gamma M + \gamma(2V^2 - \frac{17}{4}V + \frac{5}{2})}{\gamma[Z - (1-V)^2]}; \\ \frac{dV}{d \ln \xi} = (1-V)\frac{d \ln G}{d \ln \xi} - 3V + \frac{5}{2}; \\ \frac{d \ln Z}{d \ln \xi} = (\gamma - 1)\frac{d \ln G}{d \ln \xi} - \frac{5-2V-\frac{5}{2}\gamma}{1-V}; \\ \frac{dM}{d \ln \xi} = 3(G - M) \end{cases}$$

That reduces to:

$$\xi \frac{dG}{d\xi} = G \frac{\frac{3Z}{\gamma} \frac{1-\frac{5\gamma}{6}}{1-V} - \frac{17}{4}V + \frac{5}{2} + 2V^2 - \frac{25}{72}M}{Z - (1-V)^2}, \quad \xi \frac{dM}{d\xi} = 3(G - M), \quad (28)$$

$$\xi \frac{dV}{d\xi} = \xi \frac{1-V}{G} \frac{dG}{d\xi} - 3(V - \frac{5}{6}), \quad \frac{\xi}{Z} \frac{dZ}{d\xi} = \xi \frac{\gamma - 1}{G} \frac{dG}{d\xi} - \frac{5 - 2V - \frac{5}{2}\gamma}{1-V}.$$

Let us note that the expression (21) for $M(\xi)$ is also valid for the exact numerical solution. This system is solved numerically, starting from the point $\xi = 1$, where the variables are found from the conditions at the shock (8), as

$$\begin{aligned} \left. \frac{dV}{d\xi} \right|_{\xi=1} &= \frac{-30\gamma^2 - 11\gamma + 27}{6(\gamma + 1)^2}; & \left. \frac{dG}{d\xi} \right|_{\xi=1} &= \frac{-30\gamma^2 - 5\gamma + 33}{(\gamma - 1)^2}; \\ \left. \frac{dZ}{d\xi} \right|_{\xi=1} &= -\frac{\gamma(15\gamma^3 - 35\gamma^2 - 17\gamma + 49)}{18(\gamma + 1)^3}; & \left. \frac{dM}{d\xi} \right|_{\xi=1} &= \frac{6}{\gamma - 1} \end{aligned} \quad (29)$$

The sign of derivatives V' , G' and Z' is negative at $\xi = 1$, what differs from the sign of some derivatives in the approximate analytic solution in (26). It follows from the numerical integration of the system (28), that close to the shock boundary the values of $G(\xi)$ and $V(\xi)$ reach their maxima, and after decrease monotonically until the origin $\xi = 0$, see Figs.(12)-(14). Numerical solutions for $Z(\xi)$ and $M(\xi)$ for different γ are given in Figs.(15)-(16), respectively. The solutions of self-similar equations without empty voids exist only in the interval $1 < \gamma < \gamma_{**}$, where

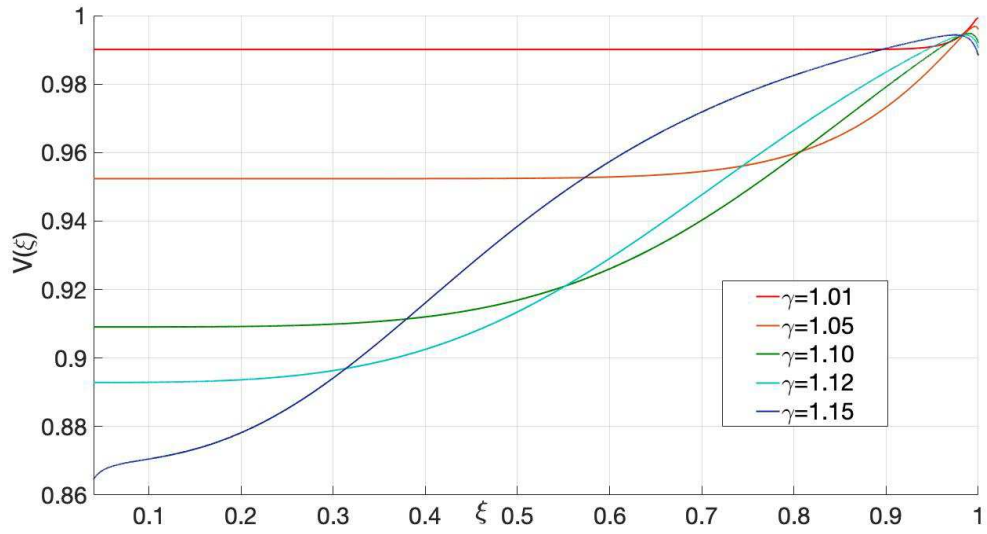


Figure 12: Numerical solution for $V(\xi)$.

$\gamma_{**} = 1.155$. At $\gamma > \gamma_{**} = 1.155$ the empty spherical void is formed around the center, at a finite distance from the shock. Similar voids are formed in Sedov solution for a shock in the static uniform gas at $\gamma > 7$ [19].

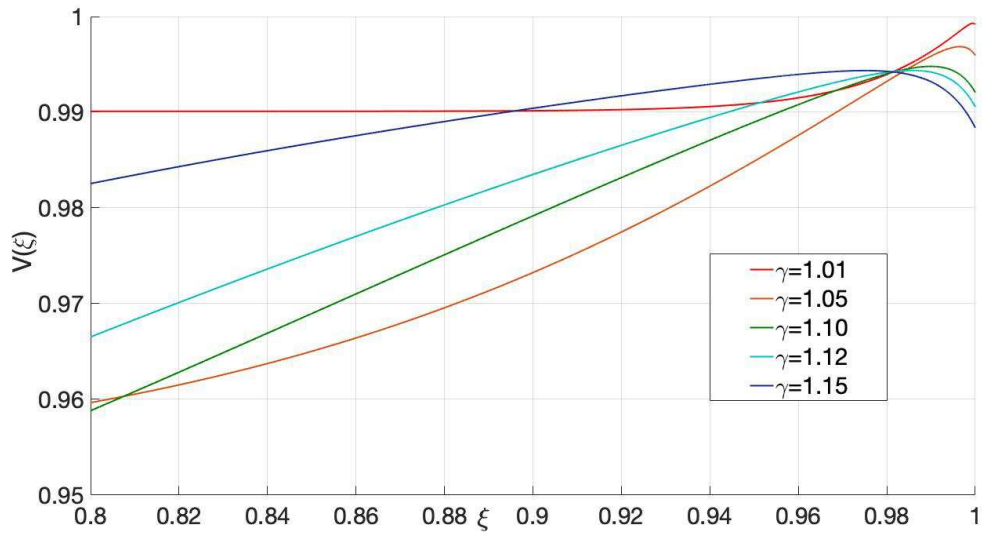


Figure 13: Numerical solution for $V(\xi)$ at ξ from 0.8 to 1.0.

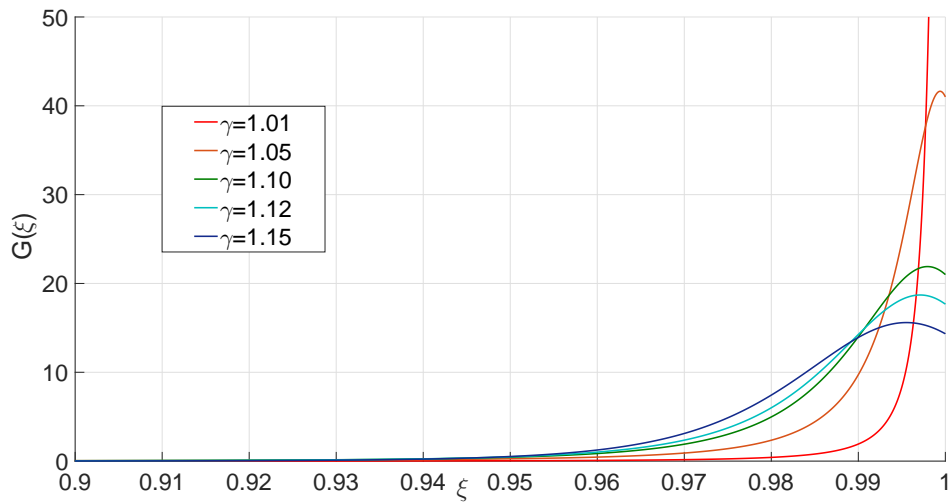


Figure 14: Numerical solution for $G(\xi)$ at ξ from 0.9 to 1.0.

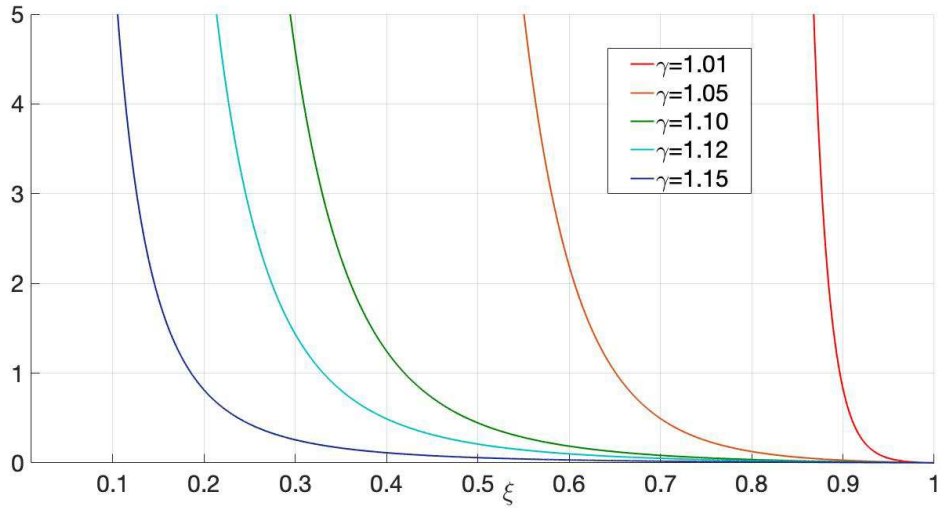


Figure 15: Numerical solution for $Z(\xi)$.

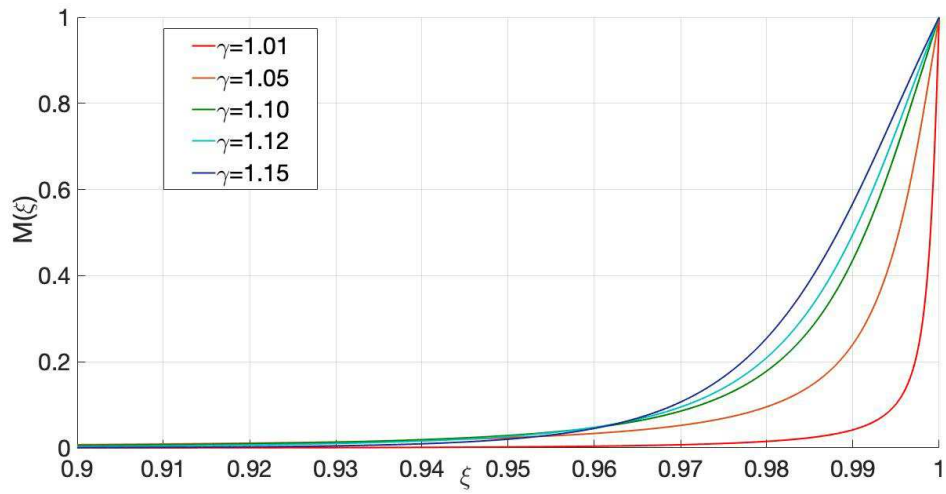


Figure 16: Numerical solution for $M(\xi)$ at ξ from 0.9 to 1.0.

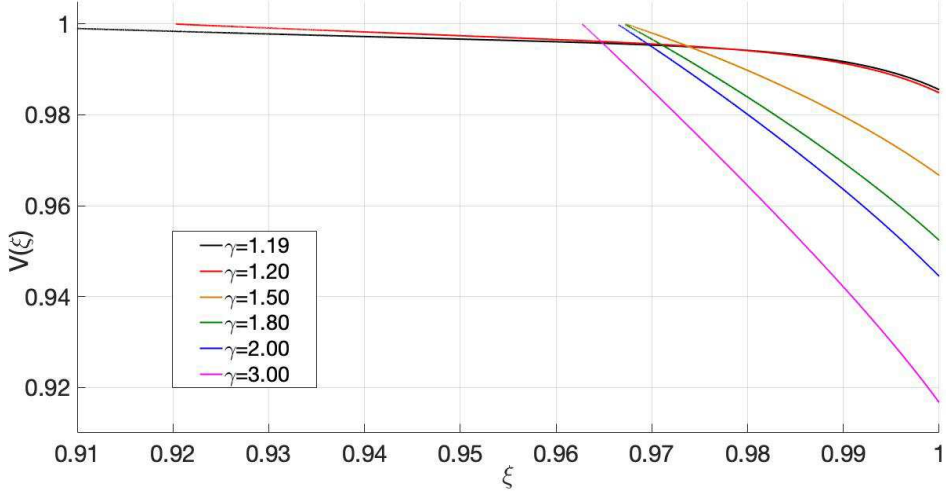


Figure 17: Numerical solution for $V(\xi)$ at big γ , at ξ from 0.91 to 1.0.

5.2 Numerical solution at γ bigger than critical value

Consider approximate analytic solution at $\gamma \geq \gamma_{**} \approx 1.155$. Like in approximate analytic solution, we consider radius of a spherical void as point where velocity $V = 1$. Such point is also a point where numerical solution stops its existence.

The important parameter is the pressure value $P \sim \rho c^2 \sim G(\xi)Z(\xi)$ at the point at $V(\xi) = 1$.

Calculations give that the pressure equals 0 at $V = 1$, but the behaviour of the density $G(\xi)$ at $V = 1$ depends on γ . Like in the approximate analytic solution, at the point with $V = 1$ the density goes to zero at $\gamma < \gamma_{cr1} = 1.4$, and for larger γ the density tends to infinity at this point. Nevertheless, the temperature goes to zero at this point, so that the pressure, represented by the function GZ goes to zero at the inner edge of the layer at $V = 1$. So we obtain a continuous pressure, self-consistent solution with a spherical void, with zero, or infinite density on its inner zero-pressure boundary. The following figures represent behaviour of functions at different $\gamma > \gamma_*$: $V(\xi)$ in Fig.(17); $G(\xi)$ in Fig.(18); $Z(\xi)$ in Fig.(19); $M(\xi)$ in Fig.(20); $G(\xi) \times Z(\xi)$ in Fig.(21).

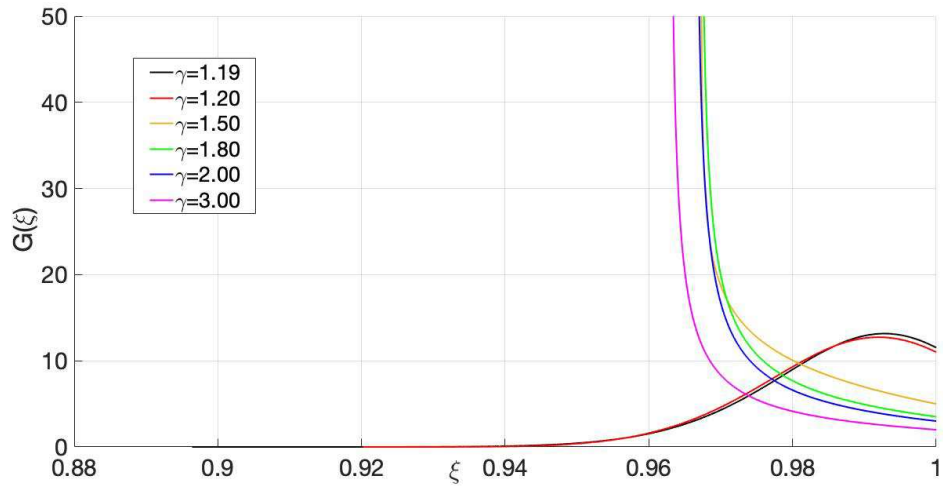


Figure 18: Numerical solution for $G(\xi)$ at big γ , at ξ from 0.88 to 1.0.

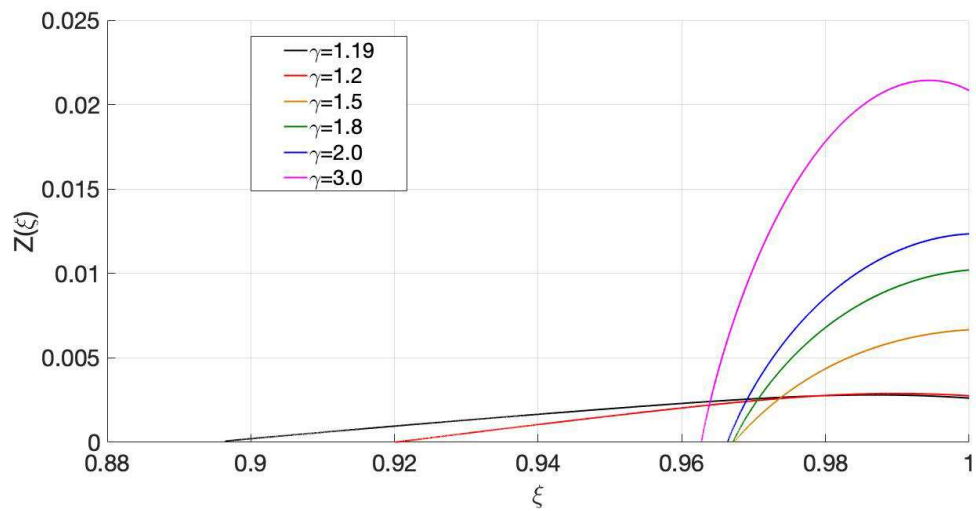


Figure 19: Numerical solution for $Z(\xi)$ at big γ , at ξ from 0.88 to 1.0.

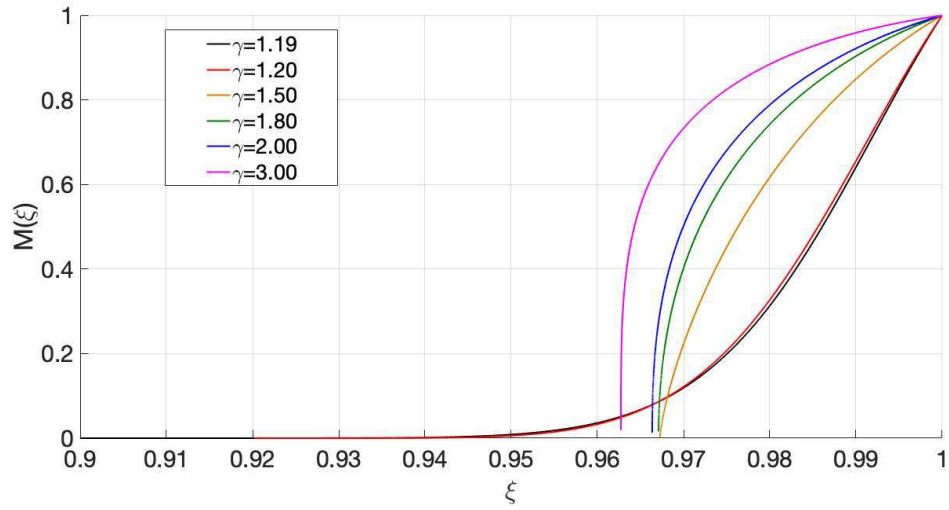


Figure 20: Numerical solution for $M(\xi)$ at big γ , at ξ from 0.9 to 1.0.

It is clear from Fig.(21), that on the inner boundary of the layer $P = 0$ due to zero temperature. Inside there is an empty hole. The density at the inner boundary at $\gamma > 1.4$ becomes infinite instead of zero at smaller ones.

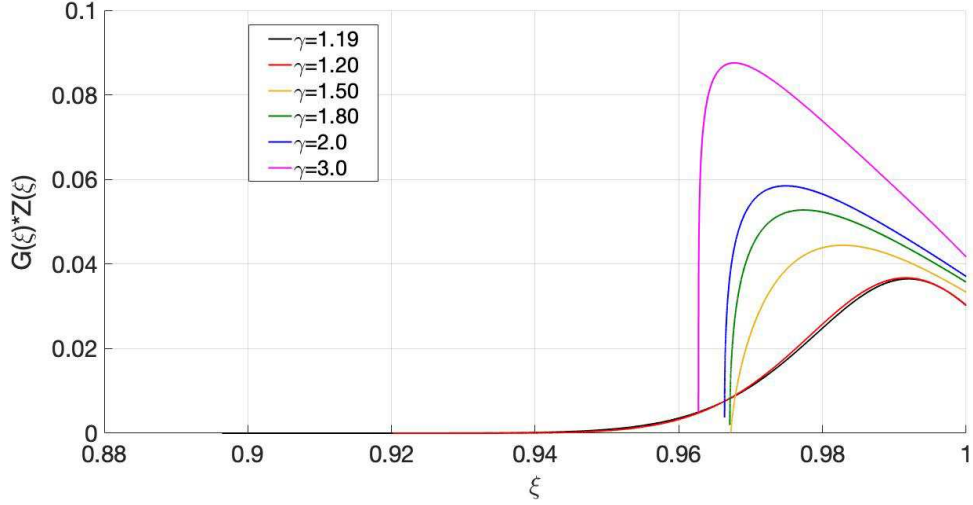


Figure 21: Numerical solution for $G(\xi) * Z(\xi)$ at big γ , at ξ from 0.9 to 1.0.

6 Comparison of approximate analytic and numerical solutions. Discussion

Let us compare radiuses of spherical void area in analytic (ξ_*^{an}) and numerical (ξ_*^{num}) solutions in the Table 1. The analytic formula for the dependence ξ_*^{an} in the analytic solution is obtained from (17) at $V = 1$. We have

$$\xi_*^{an} = \frac{(\gamma + 1)^{\mu_1 + \mu_2 + \mu_3}}{2^{\mu_1}} \left(\frac{18\gamma - 21}{15\gamma^2 + \gamma - 22} \right)^{\mu_3}, \quad (30)$$

with powers from (18) as

$$\begin{aligned} \mu_1 &= \frac{2}{15\gamma - 20}, & \mu_1 + \mu_2 + \mu_3 &= -\frac{\gamma + 1}{3\gamma - 1}, \\ \mu_3 &= -\frac{\gamma + 1}{3\gamma - 1} - \frac{\gamma - 1}{17\gamma - 15\gamma^2 + 1} + \frac{2}{20 - 15\gamma}. \end{aligned} \quad (31)$$

Tending formally $\gamma \rightarrow \infty$ we obtain from (30),(30) the value

$$\xi_*^{an}(\infty) = \left(\frac{5}{6} \right)^{1/3} = 0.941. \quad (32)$$

Table 1: The values $\xi_*(\gamma)$ for approximate analytic and numerical solutions

γ	ξ_*^{an}	ξ_*^{num}
1,18	0,2498	0,8462
1,20	0,7364	0,92018
1,50	0,938	0,9672
2,00	0,94898	0,9664
5,00	0,95084	0,9581
10,00	0,94866	0,9527

We see from the Table 1 the value of ξ_* has its maximum value both in analytic and numerical models. It indicates the thickness of the layer goes through the minimum. For $\gamma = 10$ the value of ξ_*^{an} is close to its limiting value in (32). Actually the results for large $\gamma > \sim 5$, which is obtained from self-similar solution, are not reliable. At large γ the matter compressibility decreases, and the shock is becoming weaker. Hugoniot relations in the form (5) describing the strong shock are not valid anymore. With general Hugoniot adiabatic relations [19] we cannot construct a self-similar solution. Therefore the results for large γ could be considered only as rough estimations by the order of magnitude. The maximum value of (ξ_*^{num}) in the Table 1 is related to the minimal thickness of the layer for large γ .

It may be seen from Fig. 22 that approximate analytical solution for $G(\xi)$ shows all principal layer behavior features. So it is possible to use approximate solution for different estimations.

We have made the high precision calculation and got the results, which are shown in Figs. 23,24. As we can see the density at the inner edge of the layer is jumping from zero to infinity. Comparing of these figures we have made a conclusion the transition value γ_{cr1} is equal to 1.4 at the precision of calculations.

The constant β in the definition of the non-dimensional radius ξ in (6) is obtained from the explosion energy integral E . Due to zero energy (kinetic + gravitational) in the non-perturbed solution the conserving value of the explosion energy behind the shock in the uniformly expanding medium with velocity and density distributions (2) with account of the gravitational energy determined in (14)

In non-dimensional variables (6) this relation for solutions with hollow center reduces to the equation for the constant β

$$\beta^{-5} = \frac{64\pi}{25} \int_{\xi_*}^1 G \left[\frac{V^2}{2} + \frac{Z}{\gamma(\gamma-1)} \right] \xi^4 d\xi - \frac{8}{3} \int_{\xi_*}^1 G \xi \left(\int_0^\xi G \eta^2 d\eta \right) d\xi. \quad (33)$$

Table 2: The values $\beta(\gamma)$ for the analytic and numerical solutions

γ	β_{an}	β_{num}
1.05	3.2910	3.3512
1.10	2.2268	2.5003
1.12	2.0423	2.3713
1.15	1.8522	2.2416
1.17	1.7631	2.1785
1.20	1.6667	2.1041
1.35	1.4604	1.8897
1.45	1.4048	1.8050
1.60	1.3554	1.6709
2.00	1.2814	1.1298

The values of $\beta(\gamma)$ for the analytic and numerical solutions are given in the Table 2. It follows from numbers in this table, that the value of ξ_* has its maximum value both in analytic and numerical models. It means that the thickness of the layer goes through the minimum. For $\gamma = 10$ the value of ξ_*^{an} is close to its limiting value in (32). Actually the results for large $\gamma > \sim 5$, which are obtained from self-

similar solution, are not reliable. At large γ the matter compressibility decreases, and the shock is becoming weaker. Hugoniot relations in the form (5) describing the strong shock are not valid anymore. With general Hugoniot adiabatic relations [19] we cannot construct a self-similar solution. Therefore the results for large γ could be considered only as rough estimations by the order of magnitude.

The high precision calculation for the case of γ around 1.4, gave the results, which are shown in Figs. 23,24. As we can see the density at the inner edge of the layer is jumping from zero to infinity. Comparing these figures we derive the transition value of γ_{cr1} is equal to 1.4 in both solutions, within the precision of calculations.

Acknowledgments

This work was partially supported by RFBR grants 18-02-00619, 18-29-21021 and 20-02-00455.

References

- [1] N. Tanvir (2013); arXiv:1307.6156v1.
- [2] K.P. Stanyukovich, *Nonstationary motion of continuous media. Gostekhizdat*. Moscow, (1955) (in Russian).
- [3] G.I. Taylor, Proc. Roy. Soc. **A201**, 175 (1950).
- [4] L.I. Sedov, Doklady Acad. USSR **52**, No.1 (1946).
- [5] L.I. Sedov, *Metody podobiya i razmernostei v mekhanike*. Nauka, Moscow, (1977) (in Russian).
- [6] G.S. Bisnovaty-Kogan, Gravitation and Cosmology **21**, 236 (2015); arXiv:1408.1981v2.

- [7] Ya.B. Zeldovich, I.D. Novikov, *Relativistic astrophysics. Volume 2. The structure and evolution of the universe*. Chicago, IL, University of Chicago Press (1983).
- [8] E. Bertschinger, *Astrophys. J.* **268**, 17 (1983).
- [9] I.G. Kovalenko, P.A. Sokolov, *Astron. Astrophys.* **270**, 1 (1993).
- [10] M.A. Eremin, I.G. Kovalenko, *Astron. Astrophys.* **335**, 370 (1998).
- [11] S. Ikeuchi, K. Tomisaka, J.P. Ostriker, *Astrophys. J.* **265**, 583 (1983).
- [12] L.M. Ozernoi, V.V. Chernomordik, *Soviet Astronomy*, **22**, 141 (1978).
- [13] J. Shwarz, J.P. Ostriker, A. Yahil, *Astrophys. J.*, **202**, 1 (1975).
- [14] E.T. Vishniac, J.P. Ostriker, E. Bertschinger, *Astrophys. J.* **291**, 399 (1985).
- [15] J.P. Ostriker, C.F. McKee *Astrophysical blast waves* (1988) *Rev. Modern. Physics* **60**, 1.
- [16] E. Bertschinger, *Astrophys. J.* **295**, 1 (1985).
- [17] Ya.M. Kazhdan, *Sov. Astron.* **30**, 261 (1986).
- [18] L. Ciotti, A. D’Ercole, *Astron. Astrophys.* **215**, 347 (1989).
- [19] L.D. Landau, E.M. Lifshitz, *Hydrodynamics*. Nauka, Moscow, (1988) (in Russian)
- [20] G.S. Bisnovaty-Kogan, S.A. Panafidina, *Astron. Reports* **63**, 263 (2019).

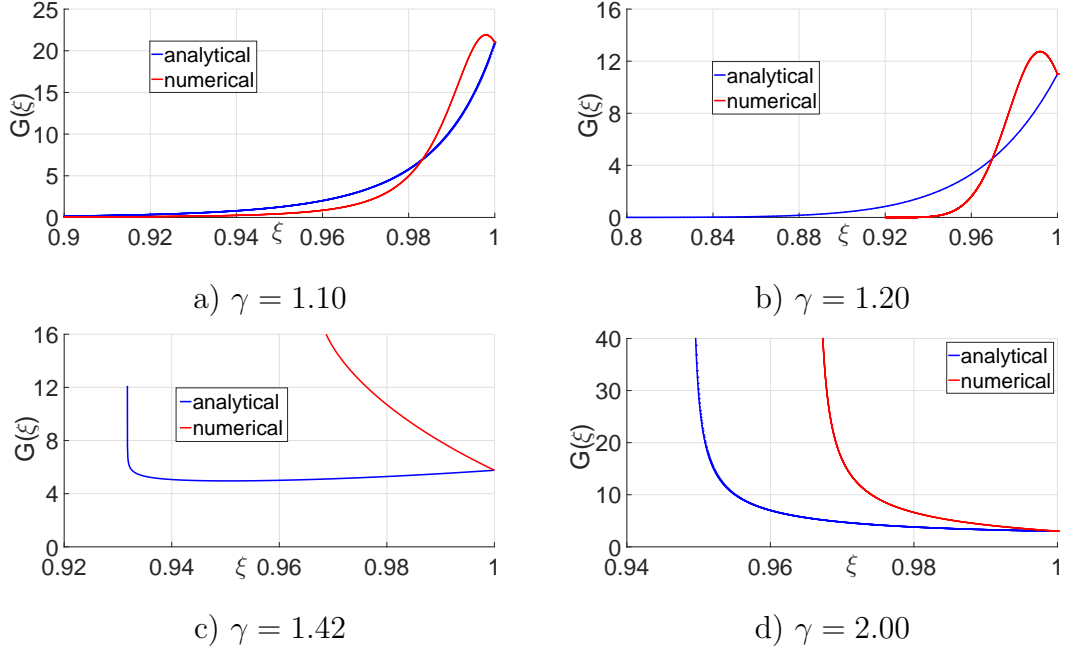


Figure 22: Comparison of analytic and numerical curves for $G(\xi)$ at different γ , in the vicinity of the shock. **a.** Example of the case without void, at $1 < \gamma < 1.1782$ (analytic); $1 < \gamma < 1.155$ (numerical). **b.** Example of the case with void, at $1.1782 < \gamma < 1.4$ (analytic); $1.155 < \gamma < 1.4$ (numerical), when the density at the edge of the void $G(\xi_*) = 0$ in both solutions. **c.** Example of the case with void, at $1.4 < \gamma < 1.543$ (analytic); $\gamma > 1.4$ (numerical), when the density at the edge of the void $G(\xi_*) = \infty$ in both solutions, and there is a minimum in the analytical curve. **d.** Example of the case with void, at $\gamma > 1.543$ (analytic); $\gamma > 1.543$ (numerical), when the density at the edge of the void $G(\xi_*) = \infty$ in both solutions, and the analytic curve does not have a minimum.

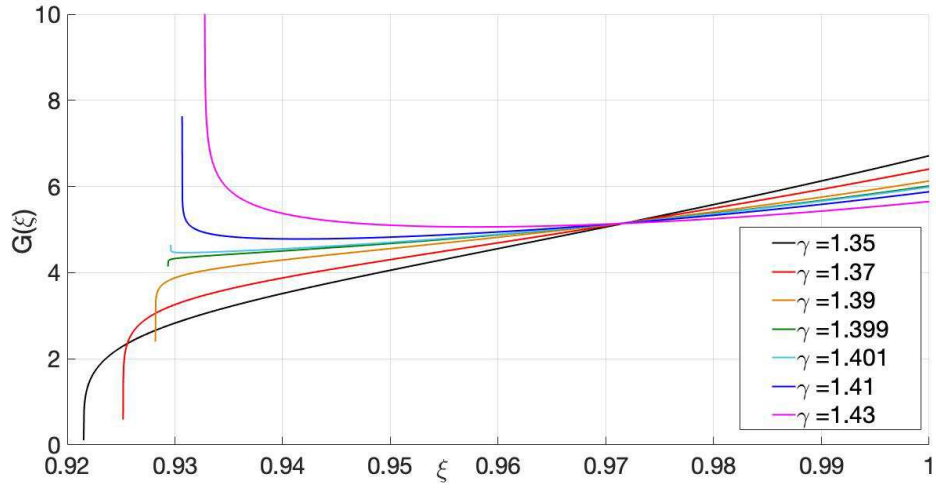


Figure 23: Approximate analytic solution for $G(\xi)$ at $\gamma \approx 1.4$

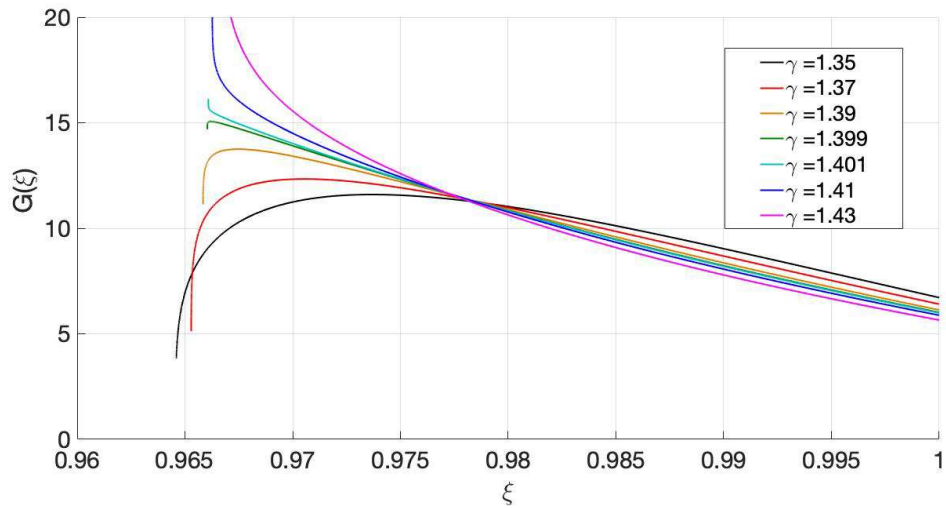


Figure 24: Numerical solution for $G(\xi)$ at $\gamma \approx 1.4$